Measuring Glassy and Viscoelastic Polymer Flow in Molecular-Scale Gaps Using a Flat Punch Mechanical Probe

Harry D. Rowland,[†] William P. King,[†,*] Graham L. W. Cross,[‡,*] and John B. Pethica[‡]

[†]Department of Mechanical Science and Engineering, University of Illinois Urbana–Champaign, Urbana, Illinois 61801, and [‡]School of Physics and Centre for Research on Adaptive Nanostructures and Nanodevices (CRANN), Trinity College, Dublin 2, Ireland

ABSTRACT This paper investigates molecular-scale polymer mechanical deformation during large-strain squeeze flow of polystyrene (PS) films, where the squeeze flow gap is close to the polymer radius of gyration (R_g). Stress–strain and creep relations were measured during flat punch indentation from an initial film thickness of 170 nm to a residual film thickness of 10 nm in the PS films, varying molecular weight (M_w) and deformation stress rate by over 2 orders of magnitude while temperatures ranged from 20 to 125 °C. In stress–strain curves exhibiting an elastic-to-plastic yield-like knee, the response was independent of M_w, as expected from bulk theory for glassy polymers. At high temperatures and long times sufficient to extinguish the yield-knee, the mechanical response M_w degeneracy was broken, but no molecular confinement effects were observed during thinning. Creep measurements in films of 44K M_w were well-approximated by bulk Newtonian no-slip flow predictions. For extrusions down to a film thickness of 10 nm, the mechanical relaxation in these polymer films scaled with temperature similar to Williams–Landel–Ferry scaling in bulk polymer. Films of 9000K M_w, extruded from an initial film thickness of $2R_g$ to a residual film thickness of $0.5R_g$, while showing stress–strain viscoelastic response similar to that of films of 900K M_w, suggestive of shear-thinning behavior, could not be matched to a constitutive flow model. In general, loading rate and magnitude influenced subsequent creep extrusion depth of high-M_w films, with deeper final extrusions for high loading rates than for low loading rates. The measurements suggest that, for high-resolution nanoimprint lithography, mold flash or final residual film thickness can be reduced for high strain and strain rate loading of high-M_w thin films.

As feature sizes in integrated circuit (IC) fabrication shrink, the demands on resists, masks, and processing equipment may render conventional lithography methods cost-prohibitive. Embossing and molding are simple techniques that may provide a route to manufacture the smallest structures. Studies have shown replication of single-walled carbon nanotubes with diameter of 2 nm *via* molding[1] and crack tips of size 0.4 nm *via* casting.[2] Nanoimprint lithography (NIL)[3] offers scalable molding of sub-10 nm features over large areas.[4] Of the various flow patterns identified in NIL,[5] squeeze-like flow has been identified as the most important in governing imprint dynamics for high-resolution molding.[5–12] As IC feature sizes shrink below 20 nm, NIL molding will extrude polymer features and residual film thickness to near or below the bulk polymer radius of gyration (R_g). The replication of molecular-scale features will require a fundamental understanding of polymer mechanical properties at the nanometer scale. Further, translating our understanding of nanoscale mechanical properties to nanomanufacturing requires an understanding of nanoscale polymer mechanical behavior in appropriate geometries and processing conditions. This paper investigates molecular-scale polymer mechanical deformation in a squeeze flow geometry, molding polystyrene (PS) films having thickness near R_g.

The properties of thin polymer films can be different from bulk polymer properties.[13,14] Recent reviews[15,16] have highlighted the influence of substrate interaction, stress history, and free surface properties on the glass transition temperature (T_g) and other modes of polymer mobility as film thickness decreases below ~100 nm.[15,16] Polymer film confinement to thickness <100 nm resulted in nonuniform T_g profiles across films,[17,18] reduced temperature dependence of viscosity,[19] and suppressed particle diffusion.[20] The most common investigations of nanometer-scale confinement effects on mechanical properties[21] are measurements of the impact of film thickness and molecular weight (M_w) on T_g of supported and freely standing PS thin films. Although there is some disagreement about the effect of confinement and M_w on T_g for supported PS thin films,[22] many independent measurements follow the empirical relation developed by Keddie and coauthors,[23] which predicts T_g reduction dependent on film thickness and independent of M_w.[24] Measurements of T_g, however, at best provide an indirect measure of chain dynamics, convoluting a time-

*Address correspondence to wpk@uiuc.edu, graham.cross@tcd.ie.

Received for review September 3, 2007 and accepted February 01, 2008.

Published online February 22, 2008.
10.1021/nn700211g CCC: $40.75

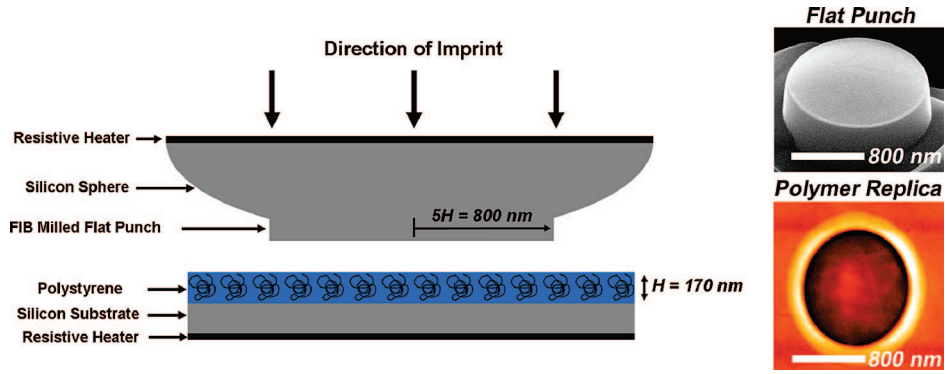

Figure 1. Illustration of squeeze flow nanomolding experiment where a flat punch mold indents a thin film of spin-cast polystyrene supported by a silicon substrate. A silicon sphere is milled by a focused ion beam (FIB) to produce the die shape shown in the SEM image, where the diameter of the flat punch is approximately 10 times larger than the polymer film thickness. An AFM scan shows the die shape replicated by imprint into polymer. The nanoimprint mold and substrate both use independent instruments for heating and thermometry.

dependent relaxation function with the temperature dependence of the average relaxation time.[21]

Only a few measurements have used a mechanical probe to measure thin-film polymer mechanical properties, and the studies have not always agreed, possibly due to differences in measurement technique and surface chemistry. Dewetting dynamics studies have investigated supported PS films, finding increasing mobility with decreasing film thickness[25] and faster hole growth rates in films of high M_w rather than low M_w.[26,27] Atomic force microscopy (AFM) measurements of biaxial creep of poly(vinyl acetate) observed rubbery regime stiffening of 26 nm films[28] rather than enhanced mobility. Numerous drainage flow studies with the surface force apparatus (SFA) have emphasized the importance of surface interactions influencing thin film mechanical properties. Polymer squeezed between strongly adsorbing surfaces showed enhanced entanglement interactions beginning at film thickness up to 5 R_g,[29] while polymer near non-adsorbing surfaces showed no enhancement of entanglement interactions down to monolayer film thickness independent of M_w.[30] The low stiffness of the mica cylinders used in SFA drainage flow studies limits the measurements to either very soft films with low M_w or melts with low T_g.[29–33] Other promising small-strain contact mechanics approaches[34] dedicated to solid film testing are emerging but remain oriented to testing below T_g and are local only in the film normal direction.

Sensitive local solid mechanics testing of thin solid-like films has been established, but the methods suffer from lack of well-defined tip geometry and limited dynamic range. For instance, in AFM nanoindentation, if the tip geometry is poorly defined, then the contact area and hence stress will be unknown, making comparison of data between different measurements problematic. The dynamic range is limited because the stiffness of the contact needs to be comparable with the cantilever stiffness to obtain adequate sensitivity. Measuring a dynamic range of material properties requires the use of multiple probes, yet the use of multiple probes exacerbates the problem of poorly defined tip contact areas.[35]

Nanoindentation testing[36] samples material at a larger scale than AFM, and the tip geometry is better defined. However, traditional nanoindentation has been limited in thin polymer films to high-modulus glassy materials due to the low stiffness of small-area contacts in low-modulus materials.[35] Furthermore, rounding defects at nanoindenter tips prohibit quantitative measurements on films thinner than the tip radius. The lack of well-defined methods suitable for measuring polymer nanomechanical properties over a wide range of temperatures and materials has resulted in measured thin-film properties seemingly dependent upon mechanical testing method. To better understand polymer mobility modes and effects of spatial confinement on polymer mobility, there is a need for fundamental mechanical property measurements of confined polymer glasses and melts for a range of materials and controlled surface conditions.

The study of polymer flow at the nanometer scale offers two challenges. The first and most fundamental challenge is to be able to make self-consistent mechanical probing measurements over a large range of deformation conditions and to identify the trends in this measurement set. The self-consistency is critical for quantitative comparison of the measurements performed at different temperatures, load rates, and molecular weights over the dimensional range of 1−1000 nm. These experiments are particularly challenging below 100 nm. The second challenge is to understand the observed phenomena in relation to bulk polymer phenomena. Continuum constitutive models of polymer mechanics are commonly used to predict polymer behavior during bulk flows, but it cannot be assumed that these models are appropriately applied to nanometer-scale polymer flows. At present, detailed knowledge of all relevant initial conditions, boundary conditions, and deformation history is not yet possible in nanoscale ex-

periments. Thus, particular care must be taken in making these comparisons. Accordingly, this study of nanometer-scale squeeze flow attempts to avoid all preconceptions as to the nature of the mechanics.

In order to address the first of these challenges, this paper presents squeeze flow measurements of supported PS thin films using a modified nanoindentation system where the indenter is a flat silicon punch.[37] The experiment features a well-defined contact area and sufficient instrument stiffness to probe dynamics of high-M_w PS during extrusions from an initial film thickness of 170 nm at temperatures below and above T_g. This new materials-testing platform[37] has full control of temperature, provides consistent geometries, and distinguishes elastic and inelastic straining processes. The technique allows quantitative stress–strain measurements of polymer thin-film squeeze flow to film thickness <10 nm, which are the conditions relevant for nanoimprint lithography.

RESULTS AND DISCUSSION

The experiments investigated polymer mechanical properties under processing conditions relevant to NIL during large-strain extrusion from an initial film thickness of 170 nm to a residual film thickness approaching 10 nm. Squeeze flow measurements probed the effect of absolute film thickness in relation to polymer R_g and M_w on glassy and viscoelastic mechanical response. The experiment measured polymer mechanical behavior above and below T_g in a squeeze-like flow geometry with a ratio of indenter diameter to initial film thickness at 10:1. Figure 1 shows the experimental setup. Indenter and substrates each used separate, independent instruments for heating and thermometry.

Polystyrene was chosen as the polymer system for several reasons. First, PS is perhaps the most widely studied polymer system in terms of thin-film polymer physics. Second, PS has been used as a model system in several studies of polymer flow during NIL.[10–12] Finally, results from measurements of PS are broadly applicable for any glass-forming polymer system. The PS films had M_w = 9000K, 900K, and 44K with expected bulk T_g = 100 °C and calculated R_g = 84, 26, and 6 nm, respectively.

Figure 2 shows representative temperature-controlled instrumented nanoimprint data illustrating the range of measurements recorded. Figure 2a shows drift-corrected load/pressure *versus* displacement curves for loading at 125 MPa/s up to 500 MPa, followed by 40 s creep at test temperatures from 20 to 125 °C. The second loading up to 900 MPa, used to determine and effectively eliminate thermal drift, can also be seen. Figure 2b presents the measurements shown in Figure 2a in another configuration, showing penetration depth *versus* time during loading. Figure 2c shows load *versus* displacement curves at 120 °C for loading at load rates from 12.5 to 1250 MPa/s.

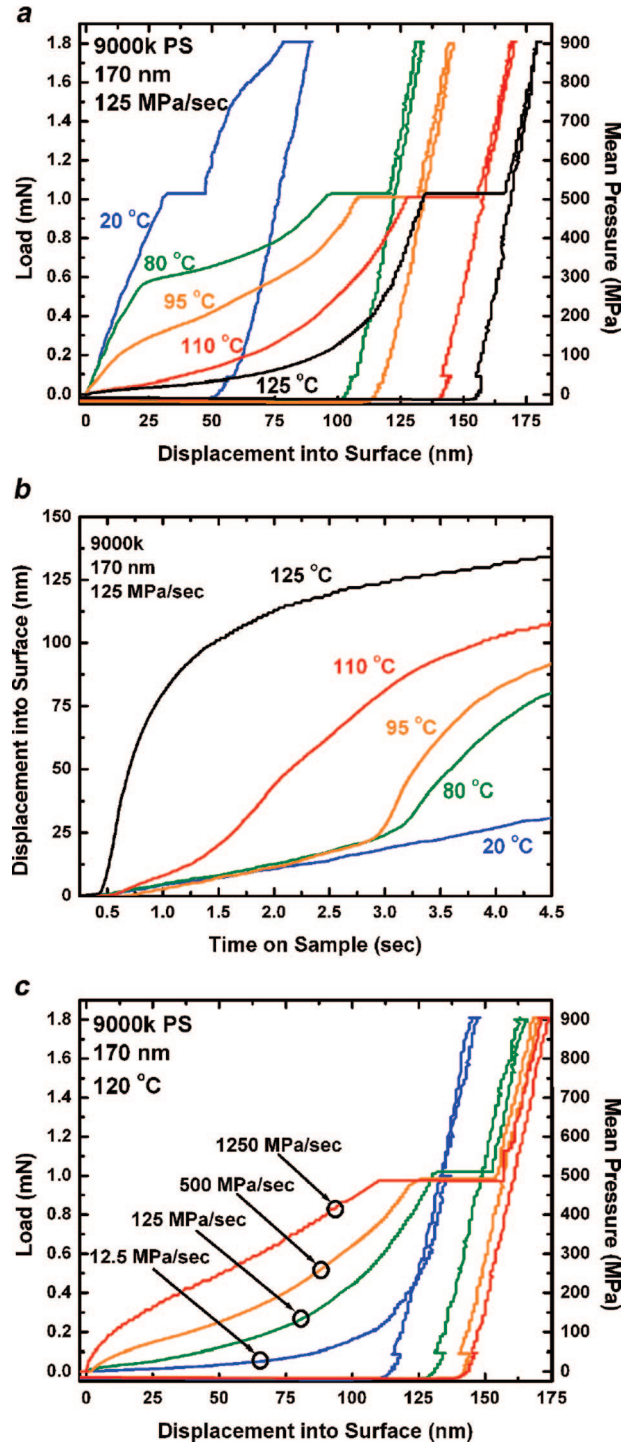

Figure 2. Load-controlled measurements molding 9000K M_w PS at 170 nm film thickness, illustrating the range of measurements recorded. (a) Load *versus* displacement measurements recorded at isothermal temperatures from 20 to 125 °C: loading at 125 MPa/s to 500 MPa, hold for 40 s to measure creep, load at 50 MPa/s to 900 MPa, hold for 40 s to measure thermal drift rates, and unload. (b) Displacement *versus* time during load at 125 MPa/s to 500 MPa. (c) Two decades of loading rates were investigated. Loading rate can modulate material response from apparent yield-free viscoelastic flow at low load rates (12.5 MPa/s) to elastic−plastic glassy behavior with post-yield flow at high load rates (1250 MPa/s).

Glass-like Mechanical Response. At any given temperature T close to or less than T_g^{bulk}, the indentation mea-

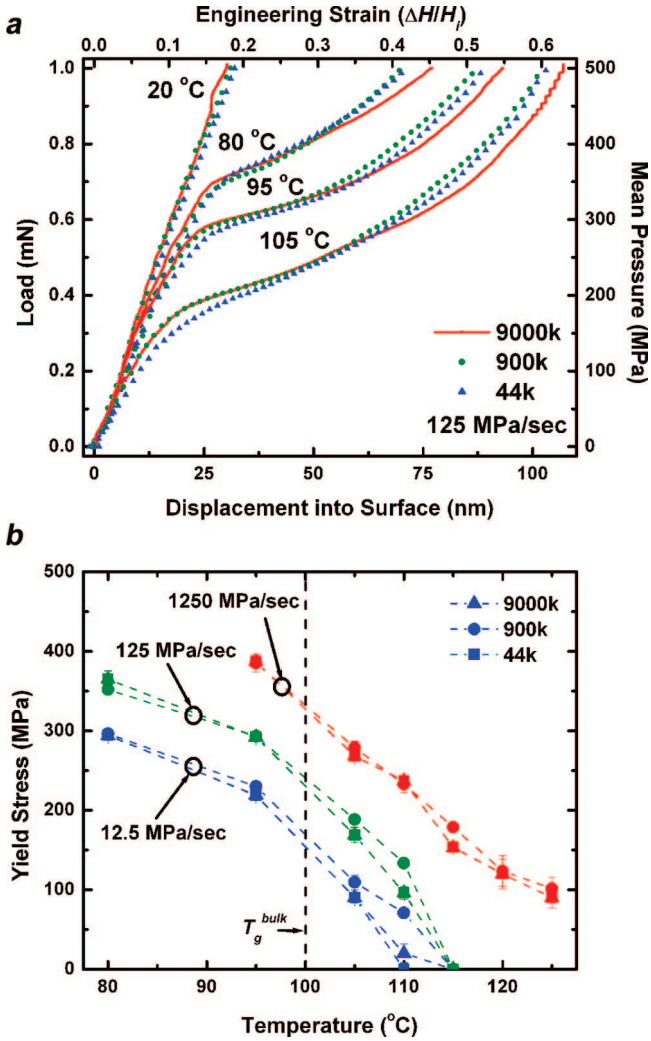

Figure 3. Glassy elastic-to-plastic transition behavior for low-polydispersity 9000K, 900K, and 44K M_w polystyrene at 170 nm film thickness. (a) Load *versus* displacement curves loading at 125 MPa/s to 500 MPa from 20 to 105 °C. A range of over two decades in molecular weight exhibits nearly identical mechanical response during loading. (b) Mean yield stress measurements loading at rates from 12.5 to 1250 MPa/s and temperatures from 20 to 125 °C. All three molecular weight films exhibit nearly identical yield stress for any observed load rate and temperature combination exhibiting the elastic-to-plastic transition.

surements in 170 nm entangled PS showed highly reproducible, glass-like stress *vs* strain response independent of M_w. Figure 3a shows load *versus* displacement curves at 125 MPa/s to 500 MPa at 20, 80, 95, and 105 °C for films of M_w = 9000K, 900K, and 44K. All three samples possessed the characteristic signature of flat punch indentation of a film of elastic−plastic material;[8] from this we infer, with increasing strain, successive regimes of recoverable (elastic) deformation, elastic-to-plastic transition at a specific yield stress, and post-yield elastoplastic flow. A yield knee was absent in all films at 20 °C up to 500 MPa load but was found in other tests to occur at about 700 MPa (see Figure 2a). The degree of congruence of the curves is remarkable, with all of the films exhibiting yield at the same elastic strain and showing identical post-yield stress increase, as expected during plastic thinning of bulk materials. Increasing temperature softened the polymer, allowing yield to occur at lower load than at room temperature. Conversely, increasing the load rate (and thus the strain rate) hardened the film response, allowing a yield knee to be observed at temperatures up to 125 °C, 25 °C above T_g^{bulk}. Figure 3b summarizes all yield stress values of the different M_w films that could be identified (within the 10 MPa stress resolution and 125 °C upper limit of the experiment) over two decades of load rate at various temperatures above 80 °C. A complete lack of molecular weight dependence (over two decades) is evident in this summary.

Viscoelastic Melt-like Mechanical Response (Yield-Free). When higher temperatures combined with slow enough loading rates extinguished the yield knee, the molecular weight degeneracy of stress *vs* strain curves also ceased to exist. In the absence of the yield knee, no fully recoverable strain region was observed in stress *vs* strain curves, and we interpret the film response to be that of a viscoelastic melt (liquid). All three molecular weight films showed qualitatively similar mechanical response, though for a given loading condition, 44K molecular weight extruded to thinner residual thickness than the higher molecular weight films. Figure 4a shows chain-length-dependent viscoelastic behavior for the three molecular weight films at 115 °C loaded at identical, slow rates of 12.5 MPa/s, increasing flow resistance (*i.e.*, viscosity) with increasing molecular weight, following the expected bulk trend. Figure 4b shows creep curves (*i.e.*, residual film thickness *vs* time) measured for the three molecular weight films at 105 and 120 °C after an initial 12.5 MPa/s loading to a penetration depth of 40 nm. Measurements near T_g^{bulk} at 105 °C, which always exhibited molecular weight independence under any testable loading condition, also showed similar creep response for all three molecular weight films. The measurements at the higher 120 °C showed similar creep response for films of 900K and 9000K molecular weight, while films of 44K are more compliant than films of higher molecular weight, as can be seen.

The amount of polymer extruded in yield-free flow was also a function of loading conditions. After long creep times, the residual film thickness of 9000K and 900K M_w below the indenter die was dependent on the initial loading-up rate, with high load rates resulting in thinner residual film thickness than low load rates. However, the residual film thickness of the 44K M_w film was independent of load rate for the highest load rates attainable here. Figure 5a,b shows load *versus* displacement curves for the 44K and 9000K M_w films at 120 °C during loading to 500 MPa with initial load-up rates ranging from 12.5 to 1250 MPa/s. In the 44K M_w film, residual film thickness after 50 s creep at 500 MPa was nearly constant, regardless of load rate. In contrast, increasing the load rate from 12.5 MPa/s to 125 or 1250

MPa/s for the 9000K M_w film decreased the residual film thickness by over 60%. Films of 900K M_w behaved like films of 9000K M_w. This enhancement of polymer displacement by initial load rate appears to require a sufficient peak stress or strain to be achieved in order to be activated. Figure 6a,b shows creep curves for the 9000K M_w film, holding load constant at 250 and 50 MPa, respectively, after loading at load rates from 12.5 to 1250 MPa/s. The initial load rate significantly influenced residual film thickness during creep at 250 MPa but had little effect when loading was limited to only 50 MPa.

In experimental conditions exhibiting a yield-free viscoelastic melt-like mechanical response, creep flow of the shortest chain length film under a modest peak load of less than 100 MPa (generating extrusions from a small initial indentation depth to a residual film thickness as small as 10 nm) can be reasonably predicted by simple viscous fluid theory. Figure 7 shows creep measurements at constant load for films of 44K M_w after loading at 125 MPa/s to an initial depth of 40 nm for temperatures from 105 to 125 °C. Solid lines in Figure 7 represent experimental measurements, and dotted lines represent least-squares curve fits for creep of a fluid with effective Newtonian viscosity under constant load. The small oscillations in creep measurements at 120 and 125 °C (Figure 7a) were instrumentation artifacts due to dynamic damping of the superimposed harmonic load. We found that a simple Newtonian fluid with a no-slip boundary condition best fit these squeeze flow creep measurements for 44K M_w,[38] as full-slip boundary conditions did not properly capture the steep change in film thickness during the initial stages of creep. The degree of agreement along the curves seemed to improve as the temperature increased. The no-slip boundary condition predicted by the curve fit is surprising, considering that bulk rheology measurements predict some amount of slip to occur above a wall shear stress of 0.1 MPa.[39]

Figure 7b shows the best-fit temperature-dependent effective Newtonian viscosity for 44K M_w to creep curves in Figure 7a along with zero shear viscosity predictions of bulk viscoelastic melt theory. The theoretical curve is the Williams–Landel–Ferry (WLF) fit to 58k M_w PS measurements of Schulz *et al.*,[11] scaled to experimental conditions by the M_w ratio to the 3.4 power. Experimental effective viscosity *versus* temperature curves from 110 to 125 °C had nearly the same slope as bulk zero shear theory, though experimental values were shifted to lower temperatures by a constant 5 °C horizontal offset from the WLF theoretical zero shear values. The 5 °C offset may be attributable to thermocouple calibration, unaccounted for elastic components of flow, hydrostatic stress influences, or thin-film polymer mobility modified from the bulk.

Creep flow in 900K and 9000K M_w films exhibiting a yield-free viscoelastic melt-like mechanical response

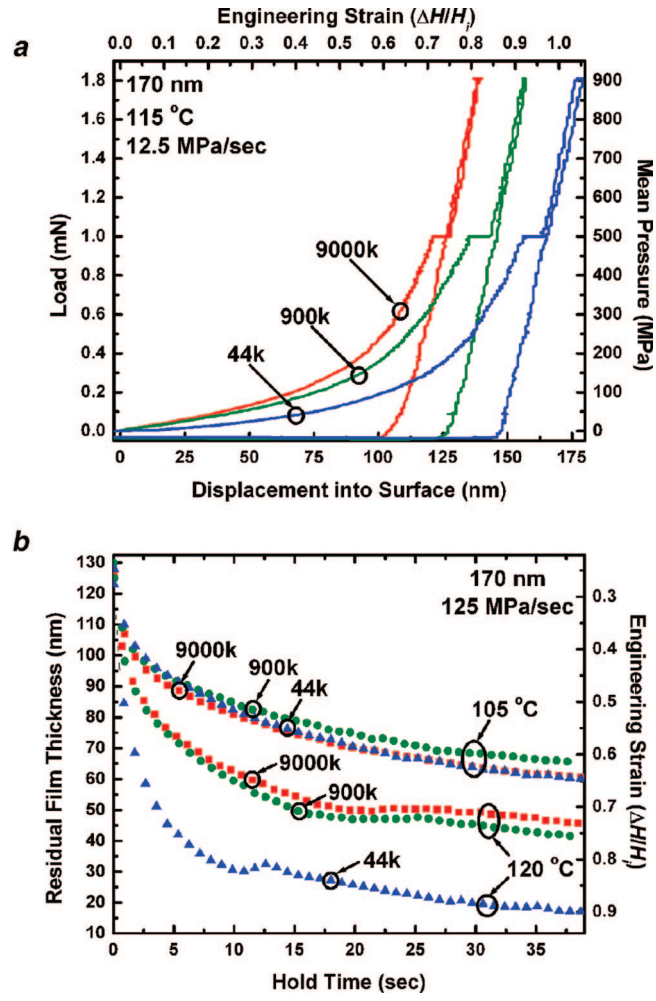

Figure 4. Chain-length-dependent viscoelastic behavior for 9000K, 900K, and 44K M_w PS at 115 °C. (a) Loading measurements show that films of 44K M_w extrude to thinner residual film thickness than films of 900K M_w, which in turn extrude to thinner residual film thickness than films of 9000K M_w. (b) Creep measurements after an initial penetration depth of 40 nm show similar response in all M_w films near T_g. At temperatures well above T_g, high-molecular-weight films of 9000K behave like films of 900K M_w, while films of 44K M_w show a more compliant response.

suggested a shear-thinning behavior governing flow, as the reptation time constants for both films were well above the experimental time scale at the temperatures investigated. No-slip power law fluid predictions, where $\eta = m\dot{\gamma}^{n-1}$, with η the shear-rate-dependent viscosity, $\dot{\gamma}$ the shear rate, and n the shear-thinning exponent, compared well to measurements in 9000K and 900K M_w films during extrusions down to 45 nm residual film thickness (measurements and predictions not shown). However, interpretation of measurements in 900K and 9000K M_w films and comparisons of the film behavior to bulk values are difficult endeavors, as the low temperatures and confined state of the films require several tenuous assumptions to fit the film behavior to one of a variety of rheological constitutive models.

Thin-film polymer mechanical properties measured here during squeeze flow extrusions in entangled poly-

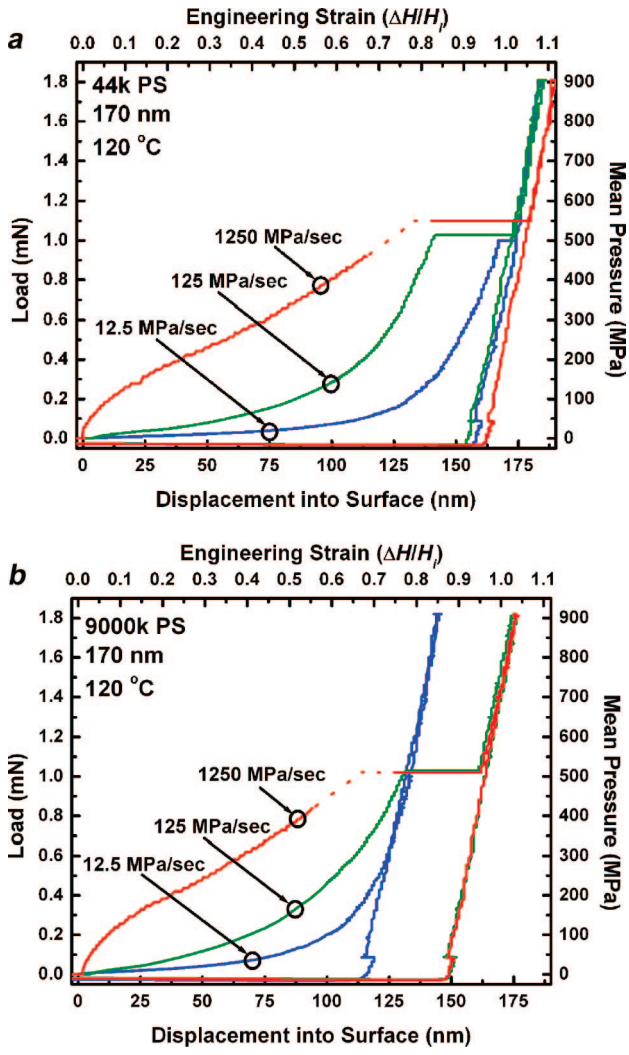

Figure 5. During creep after loading at high load rates (possibly modifying the entanglement network), deeper extrusions occur than when loading at low load rates in high-M_w polymer. (a) Load *versus* displacement curves in 44K M_w polystyrene at 120 °C loading to 500 MPa at rates from 12.5 to 1250 MPa/s. In this low-molecular-weight system, final creep depth is independent of load rate. (b) Load *versus* displacement curves in 9000K M_w at 120 °C loading to 500 MPa at rates from 12.5 to 1250 MPa/s. Here, final creep depth after loading at 125 and 1250 MPa/s is greater than final creep depth after loading at 12.5 MPa/s.

styrene systems qualitatively agree with forms that might be expected from bulk glassy and viscoelastic deformation, regardless of initial or instantaneous confinement ratio (*i.e.*, ratio of residual film thickness below punch to radius of gyration). During loading exhibiting a yield-knee, the films possess molecular-weight-independent, glass-like plasticity as expected from bulk continuum mechanics for PS; this suggests an identical nature of chain entanglement for all three films.[40,41] During yield-free loading of an apparent viscoelastic melt state, diverging stress–strain curves indicate a broken molecular weight degeneracy, as would be expected in bulk polymer, and even shorter chain films of 44K M_w seem to follow bulk viscoelastic trends. This result concurs with the M_w dependence of flow characteristics reported for nanoimprint structure relaxation studies.[42]

The M_w degeneracy remains unaffected by spatial confinement arising during extrusion from an initial film thickness of 170 nm down to ~50 nm residual film thickness. In bulk polymers, deformations in the glassy state perturb segments of polymer chain less than the entanglement spacing or tube diameter, about 5 nm in entangled PS systems. Deformations during elastic loading result from short-range molecular motions,[43] while deformations during yielding and post-yield plastic flow at small strains result in cooperative molecular motions associated with glass–rubber α transitions on the length scale of one tube diameter or smaller.[40,44–46] For the thin films measured here, elastic loading, yield stress, and post-yield plastic flow properties are identical for extrusions from an initial film thickness of 170 nm down to ~50 nm or residual film thicknesses of $0.6R_g$, $1.9R_g$, and $8.3R_g$ for films of M_w = 9000K, 900K, and 44K, respectively. These measurements suggest that short-range molecular motions are largely unaffected by initial or instantaneous confinement ratio. Additionally, these results also show that the frictional boundary condition between the indenter and films was virtually identical and not affected by chain length or particular sample preparation variations. This condition is particularly important for self-consistent measurements, where the forming stress during upset forging of squat plastic samples, as for the thin-film squeezing of these experiments, can be highly sensitive to frictional boundary conditions.[47]

Similar to bulk viscoelastic melt theory, the thin-film viscoelastic melt mechanical properties measured here are dependent on M_w, as conformational changes of extended polymer chain segments are unlocked at $T > T_g$. In bulk polymer systems, viscosity or resistance to flow depends on full chain length and scales by $M_w^{3.4}$. Although the viscoelastic properties of films of 900K and 9000K M_w are difficult to analyze in this work due to experimentally inaccessible reptation time constants, films of 44K M_w have theoretical reptation time constants less than the experimental flow time scale at 120 and 125 °C. Short-chain 44K M_w PS with M_w just above M_c = 35K behaves like a simple WLF temperature-dependent no-slip fluid with an effective Newtonian viscosity near the theoretical zero shear viscosity during extrusions from 170 to 10 nm or $1.5R_g$ film thickness. However, the experimentally determined effective viscosity for a given temperature is lower than bulk WLF zero shear theory predicts, with the measured viscosity curve shifted horizontally by 5 °C from the theoretical viscosity curve. The low effective viscosity values are surprising, considering that the high hydrostatic pressure during measurement could shrink free volume and increase flow resistance.[48] The lower effective viscosity could be due to thermocouple calibration error, partial wall slip, enhanced surface layer

mobility in thin films,[17,18] or shear-rate-dependent behavior and elastic components of flow, as seen in dewetting studies of thin films.[49] The lower effective viscosity is not likely caused solely by shear-thinning behavior, as several rheological studies show Newtonian fluid response at high shear rates for fluids of $M_W \leq M_C$.[50,51] Shear-thinning in 44K M_w PS might result in a viscosity similar to that of 35K M_w PS; however, shear-thinning would not be expected to cause observed viscosities significantly lower than the Newtonian viscosity of 35K M_w PS.

The offset between measured viscosity and WLF theoretical viscosity remains constant at 5 °C from 110 to 125 °C, indicating that the final extrusion depth, even down to 10 nm, does not influence the measured viscosity. The time–temperature scaling of the measurements suggests that WLF time–temperature scaling is also independent of initial or instantaneous confinement ratio. The self-consistent measurements for all M_w films described in this paper, during extrusions to residual film thicknesses from 10 to 60 nm at temperatures from 105 to 125 °C, suggest that the state of polymer chain entanglement given by the initial film thickness, rather than the instantaneous extruded film thickness, governs polymer mechanical properties during squeezing on time scales relevant to nanoimprint manufacturing.

We also observed that large-strain deformations at high load rates can reduce the residual film thickness of high-M_w materials during squeeze flow. Here, high strain rates force polymer melts to respond in an elastic mode (before yield ensues), deforming network constraints and entanglement orientation rather than inducing large relative motion of polymer molecules. For highly entangled systems, the deformation occurs on time scales much shorter than full-chain diffusion time constants, as structural reorganization governed by full-chain diffusion scales with $M_w^{3.4}$ at $T > T_g$. We propose that large-strain loading ≥125 MPa/s was sufficiently fast to change the mechanics of extrusions in highly entangled 9000K and 900K M_w but not in slightly entangled 44K M_w. The change in mechanics results from elastic deformation aligning the entanglement network, possibly enhancing slip at the polymer−silicon interface, with the deformation field changing from a sheared squeeze flow toward a biaxial extensional flow. Segmental alignment could also result from plastic yield processes arising from the high stresses generated, as molecular dynamics simulations suggest.[52] Holding load to perform creep after altering network constraints allows polymer relaxations to occur with enhanced flow properties. For low-M_w samples such as 44K M_w, the short polymer chains quickly relax, dissipating any elastic stresses of network strain built in during loading, and effectively resist the tendency to undergo network alteration by rapid loading. Thus, the ultimate residual film thickness following

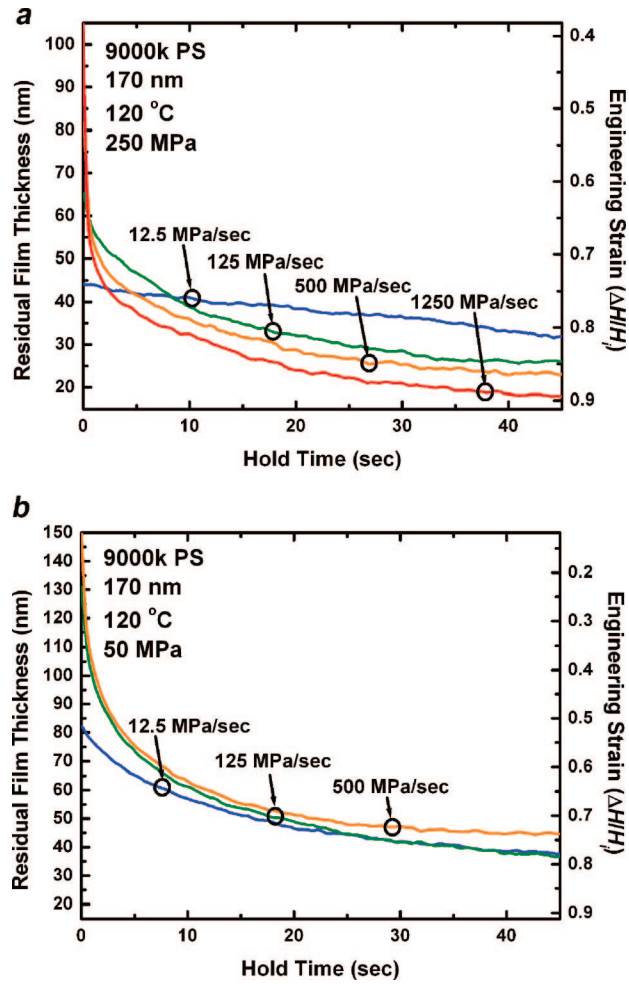

Figure 6. (a) Creep curves in 9000K M_w PS at 120 °C after loading to 250 MPa at rates from 12.5 to 1250 MPa/s. Final creep depth depends on load rate during load. (b) Creep curves in 9000K M_w PS at 120 °C after loading to 50 MPa at rates from 12.5 to 500 MPa/s. Load rate does not influence final creep depth for creep at 50 MPa.

creep after loading is independent of load rate for short-chain polymers. One is left with the surprising and technologically interesting situation that a long-chain entangled melt can be thinned equivalently to a short-chain version due to an apparent susceptibility to network conditioning by rapid loading.

Overall, the experimental results indicate new opportunities for investigating polymer flow physics at small length scales. The geometry of the flat punch probe allows quantitative comparison of stress–strain behavior in thin polymer films over the range of 10–300 nm under a wide range of mechanical conditions, which is a capability not previously available to the nanomechanics community. The quality of our results demonstrates highly consistent trends across a wide parameter set of temperature, stress rate, and molecular weight. The step of making comprehensive quantitative comparison with bulk polymer mechanics theory and experiment will be aided by establishing a rheometric flow with verified low friction boundary conditions, and ultimately nanoscopic flow field visualization techniques if they can be developed.

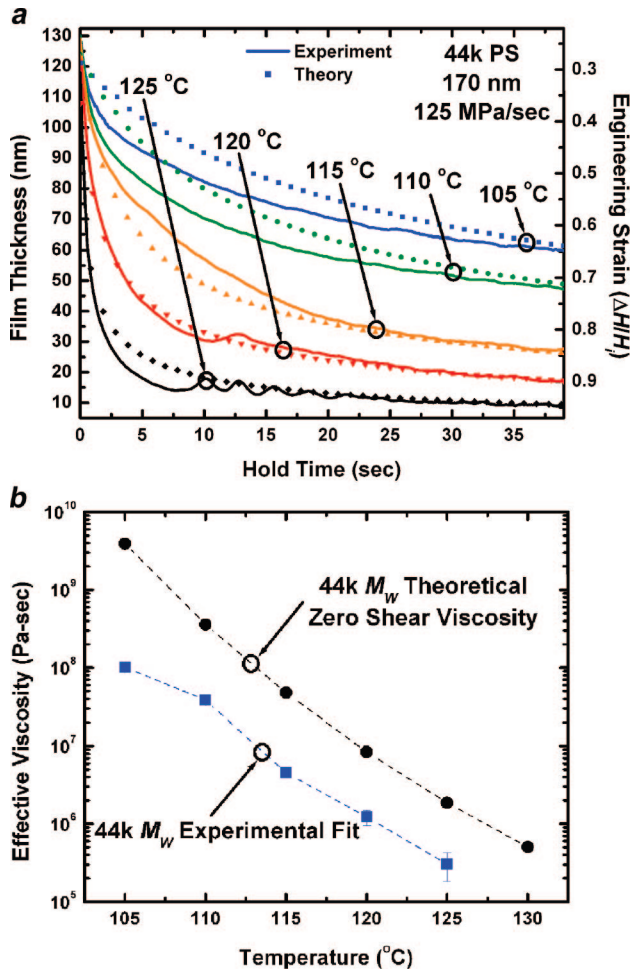

Figure 7. Bulk viscoelastic theory with no-slip boundary conditions predicts creep response of 44K M_w PS after small-strain loading. The solid lines represent measurements while the dotted lines are no-slip curve fits. (a) Creep measurements in 44K M_w and corresponding Newtonian fluid curve fits with no-slip boundary conditions. Oscillations in experimental curves are instrumental artifacts due to damping of superimposed harmonic load. (b) Best-fit Newtonian viscosity for 44K M_w as a function of temperature and corresponding Williams–Landel–Ferry (WLF) theoretical zero shear viscosity. Experiment shows a constant 5 °C offset from WLF theory.

This end may also benefit from the introduction of strain-rate-controlled deformation history. Not explicitly studied here is the effect of confinement in the thin polymer films, both above and below T_g. While in a few of the cases the polymer films are squeezed to a thickness less than the bulk radius of gyration, it would be interesting to compare stress–strain curves with polymer films in which the initial polymer film thickness is less than the bulk radius of gyration.

The results of this study provide insight into process conditions for nanoimprint lithography. As previously reported, squeeze flow between the flat tool and the hard substrate governs the dynamics of polymer flow and cavity filling during NIL.[5–12] The squeeze flow is somewhat less important for the case of a very thick polymer film and complete filling of the tool cavities.[5–7] However, for IC fabrication, or for other applications where residual polymer thickness ("mold flash") is to be reduced, the polymer flow dynamics are completely governed by long-range polymer squeeze flow.[5] This is true even for the case where there are many cavities in the tool of vastly different sizes.[7] From the present study, we can conclude that, for high-M_w films above the entanglement threshold, such as those that are most often used in NIL, high loads and high load rates can produce lower residual film thickness than low loads and low load rates.

CONCLUSION

This paper investigates molecular-scale polymer mechanical deformation during large-strain squeeze flow processing conditions relevant to nanoimprint lithography. Instrumented nanoimprint experiments probed the effect of polymer R_g and M_w on mechanical response, extruding PS films from an initial thickness of 170 nm to a residual film thickness of 10 nm. Load-displacement and creep relations were measured in 9000K, 900K, and 44K M_w PS over temperatures ranging from 20 to 125 °C and load rates from 12.5 to 1250 MPa/s.

The measurements showed that the structure of the initial film thickness, not the instantaneous residual film thickness, determines the state of polymer entanglements, with mechanical properties similar to bulk predictions for films with initial thickness $>2R_g$. The yield-free response of 44K M_w films was well-approximated by theoretical predictions from bulk, with near-WLF time–temperature scaling. Films of 9000K M_w PS, during extrusions from $2R_g$ to $0.5R_g$, behaved like films of 900K M_w PS. During large-strain extrusions of high-M_w polymer melts, high load rates resulted in thinner residual films than low load rates. The measurements suggest that, for high-M_w thin films, NIL mold flash can be reduced at high strain and high strain rate. Since it has well-defined contact area and surface interactions, NIL squeeze flow can investigate polymer physics from length scales near the polymer tube diameter to well above the polymer coil radius. Reliable large -strain mechanical testing of thin polymer films should assist the engineering of nanostructured materials and processes.

EXPERIMENTAL METHODS

Polymer Sample Preparation. Polystyrene was chosen as a representative amorphous polymer standard with well-studied film thickness dependence of T_g and non-adhering surface interactions with native silicon oxide surfaces.[23,24] Three narrow M_w distributions of PS were investigated, with two highly entangled polymeric systems and one system just above the critical entanglement molecular weight, M_c = 35K.[53] 9000K M_w PS with polydispersity index PDI = 1.22 was obtained from Polymer Source, and 900K M_w PS with PDI = 1.10

and 44K M_w PS with PDI = 1.07 were obtained from Scientific Polymer.

It is understood that thin-film polymer preparation techniques may be the source of conflicting results between various reports. In our experiments, thin films were prepared to a thickness of 170 ± 3 nm by spin-casting dilute solutions of PS in toluene onto lithographic-grade polished silicon wafers. Wafers were initially cleaned by acetone, methanol, and deionized water rinse, followed by a 20 min dehydration bake at 120 °C. PS samples were annealed at 150 °C for 120 min in air to reduce spin-casting-induced internal stresses,[54] with heating and cooling ramps <5 °C/min, holding the temperature for 15 min every 25 °C increment. PS samples were aged for 5 months at 20 °C prior to testing and showed no signs of large-scale dewetting. A Woollam M-2000 ellipsometer measured the resulting film thickness with standard deviation <5.0 nm.

Instrumented Nanoimprint Setup. A commercial nanoindentation system, Nanoindenter XP from MTS Systems, embossed the polymer films. Details of the modifications to the nanoindentation system for temperature-controlled squeeze flow embossing are described elsewhere[37] and only briefly summarized here. The nanoindenter system is capable of displacement sensing with precision <1 nm. Focused ion-beam milling shaped a 1 mm diameter polished single-crystal silicon sphere (roughness ~2 nm rms) nanoindenter tool into a flat punch of height 550 ± 100 nm and diameter 1600 ± 50 nm. Surface mount resistors and a thermocouple were epoxied to the silicon sphere. Silicon-supported PS samples were fixed to a thermoelectric heater, and a thermocouple was mounted 2 mm from the PS samples. The heater was glued to thermally insulating ceramic fixed to a tilt stage. All PS samples were aligned to the flat punch silicon molds to less than 0.1°, as measured by *in situ* AFM imaging of the shallowest flat punch replications into the polymer. Thermocouples were calibrated to within 0.1 °C. The temperature-controlled instrumented nanoimprint measurements were performed at temperatures from 20 to 125 °C. With stringent alignment,[37] the measurements deviate slightly from true squeeze flow and uniaxial compression tests due to edge constraint of surrounding film, but the large aspect ratio of the tool diameter to film thickness and the high pressure between the nanoimprint tool and substrate reduces the influence of edge effects on measured properties.[55,56] With full-slip boundary conditions, the measurements closely approximate uniaxial compression.

Measurements. Measurements were performed under direct current loading control. A superimposed alternating current modulation[57] provided an additional 45 Hz sinusoidal loading; this was feedback regulated throughout the test to provide a constant 2 nm vertical amplitude oscillation. Both the amplitude and phase of the resulting alternating current displacement were recorded. The oscillatory load enabled sensitive detection of the initial mold/surface contact to within 2 nm, as well as dynamic stiffness measurement.[57] All tests followed an identical five-part loading history: (1) Detect arrival of mold at surface and then load at constant load rate to predetermined load or depth. (2) Hold load and allow creep for 40–50 s. (3) Load at 50 MPa/s to 900 MPa. (4) Hold load for 20−25 s to allow high load creep to cease and then hold load for 20–25 s to measure thermal drift displacement rate. (5) Unload at 50 MPa/s to 50 MPa, hold for 10 s, and then unload at slow load rate of 12.5 MPa/s to minimize adhesion upon demolding. Due to the constant contact area, load is readily converted to mean contact pressure. Likewise, loading rates of change directly determine contact pressure rates of change. Over two decades of loading rates were tested between 12.5 and 1250 MPa/s. Three identical tests were recorded for each loading condition at virgin sample locations precisely separated by 7 μm.

For non-room-temperature testing, PS samples were heated at 1 °C/min and held at 80 °C overnight for temperature equilibration. Indenter and stage thermocouples were calibrated at 80 °C by sweeping the power applied to the nanoimprint mold resistors such that the temperature of the nanoimprint mold did not change during approach and retraction from the sample. Critically, this indicated isothermal contact conditions at the stage temperature.[37] Measurements were made at temperatures up to 125 °C after heating at 1 °C/min and holding the desired temperature for 30 min per 5 °C heating increment to allow thermal equilibration. Thermal drift displacement rates were <0.25 nm/s for all temperatures.

The influence of sample preparation on glassy properties was tested by recording measurements in the glassy state after controlled heating and cooling above T_g. Minimal changes in mechanical response before and after heating above T_g indicated only a slight influence of physical aging due to sample preparation. Molds were cleaned for 15 min with oxygen plasma before testing pristine PS samples. The oxygen plasma slightly etched the molds, rounding the mold edges after multiple cleanings. However, measurements on identical materials before and after multiple cleanings showed no discernible change in mechanical signal.

Acknowledgment. The authors are grateful for support from the Science Foundation of Ireland Grant C028, NSF CMMI 07-32114, The Center for Nanoscale Chemical-Electro-Mechanical Manufacturing Systems (Nano-CEMMS), NSF DMI 03-28162, NSF CAREER CBET 07-31930, and DOE PECASE.

REFERENCES AND NOTES

1. Hua, F.; Sun, Y.; Gaur, A.; Meitl, M. A.; Bilhaut, L.; Rotkina, L.; Wang, J.; Geil, P.; Shim, M.; Rogers, J. A. Polymer Imprint Lithography with Molecular-Scale Resolution. *Nano Lett.* **2004**, *4*, 2467–2471.
2. Xu, Q.; Mayers, B. T.; Lahav, M.; Vezenov, D. V.; Whitesides, G. M. Approaching Zero: Using Fractured Crystals in Metrology for Replica Molding. *J. Am. Chem. Soc.* **2005**, *127*, 854–855.
3. Chou, S. Y.; Krauss, P. R.; Renstrom, P. J. Imprint of sub-25 nm Vias and Trenches in Polymers. *Appl. Phys. Lett.* **1995**, *67*, 3114–3116.
4. Khang, D.; Lee, H. Wafer-Scale Sub-Micron Lithography. *Appl. Phys. Lett.* **1999**, *75*, 2599–2601.
5. Rowland, H. D.; King, W. P.; Sun, A. C.; Schunk, P. R. Impact of Polymer Film Thickness and Cavity Size on Polymer Flow During Embossing: Toward Process Design Rules for Nanoimprint Lithography. *J. Micromech. Microeng.* **2005**, *15*, 2414–2425.
6. Rowland, H. D.; King, W. P. Polymer Deformation and Filling Modes during Microembossing. *J. Micromech. Microeng.* **2004**, *14*, 1625–1632.
7. Rowland, H. D.; King, W. P.; Sun, A. C.; Schunk, P. R. Simulations of Nonuniform Embossing: The Effect of Asymmetric Neighbor Cavities on Polymer Flow during Nanoimprint Lithography. *J. Vac. Sci. Technol. B* **2005**, *23*, 2958–2962.
8. Cross, G. L. W.; O'Connell, B. S.; Pethica, J. B. Influence of Elastic Strains on the Mask Ratio in Glassy Polymer Nanoimprint. *Appl. Phys. Lett.* **2005**, *86*, 081902.
9. Cross, G. L. W. The Production of Nanostructures by Mechanical Forming. *J. Phys. D: Appl. Phys.* **2006**, *39*, R363–R386.
10. Schulz, H.; Wissen, M.; Scheer, H. C. Local Mass Transport and its Effect on Global Pattern Replication during Hot Embossing. *Microelectron. Eng.* **2003**, *67–68*, 657–663.
11. Schulz, H.; Wissen, M.; Bogdanski, N.; Scheer, H. C.; Mattes, K.; Friedrich, C. Choice of the Molecular Weight of an Imprint Polymer for Hot Embossing Lithography. *Microelectron. Eng.* **2005**, *78–79*, 625–632.
12. Schulz, H.; Wissen, M.; Bogdanski, N.; Scheer, H. C.; Mattes, K.; Friedrich, C. Impact of Molecular Weight of Polymers and Shear Rate Effects for Nanoimprint Lithography. *Microelectron. Eng.* **2006**, *83*, 259–280.
13. De Gennes, P. G. *Scaling Concepts in Polymer Physics*; Cornell University Press: Ithaca, NY, 1979; p 324.
14. Jones, R. L.; Kumar, S.; Ho, D. L.; Briber, R. M.; Russell, T. Chain Conformation in Ultrathin Polymer Films. *Nature* **1999**, *400*, 146–149.
15. Alcoutlabi, M.; McKenna, G. B. Effects of Confinement on Material Behaviour at the Nanometre Size Scale. *J. Phys.: Condens. Matter* **2005**, *17*, R461–R524.
16. Granick, S.; Kumar, S.; Arnis, E.; Antonietti, M.; Balazs, A.; Chakraborty, A.; Grest, G.; Hawker, C.; Janmey, P.; Kramer,

E.; *et al.* Macromolecules at Surfaces: Research challenges and Opportunities from Tribology to Biology. *J. Polym. Sci. B—Polym. Phys.* **2003**, *41*, 2755–2793.
17. Ellison, C. J.; Torkelson, J. M. The Distribution of Glass-Transition Temperatures in Nanoscopically Confined Glass Formers. *Nat. Mater.* **2003**, *2*, 695–700.
18. Sills, S.; Overney, R. M.; Chau, W.; Lee, V. Y.; Miller, R. D.; Frommer, J. Interfacial Glass Transition Profiles in Ultrathin, Spin Cast Polymer Films. *J. Chem. Phys.* **2004**, *120*, 5334–5338.
19. Li, C.; Koga, T.; Li, C.; Jiang, J.; Sharma, S.; Narayanan, S.; Lurio, L. B.; Hu, X.; Jiao, X.; Sinha, S. K.; *et al.* Viscosity Measurements of Very Thin Polymer Films. *Macromolecules* **2005**, *38*, 5144–5151.
20. Frank, B.; Gast, A. P.; Russell, T.; Brown, H. R.; Hawker, C. Polymer Mobility in Thin Films. *Macromolecules* **1996**, *29*, 6531–6534.
21. Forrest, J. A. A Decade of Dynamics in Thin Films of Polystyrene: Where Are We Now? *Eur. Phys. J. E* **2002**, *8*, 261–266.
22. Singh, L.; Ludovice, P. J.; Henderson, C. L. Influence of Molecular Weight and Film Thickness on the Glass Transition Temperature and Coefficient of Thermal Expansion of Supported Ultrathin Polymer Films. *Thin Solid Films* **2004**, *449*, 231–241.
23. Keddie, J. L.; Jones, R. A. L.; Cory, R. A. Size-Dependent Depression of the Glass-Transition Temperature in Polymer-Films. *Europhys. Lett.* **1994**, *27*, 59–64.
24. Ellison, C. J.; Mundra, M. K.; Torkelson, J. M. Impacts of Polystyrene Molecular Weight and Modification to the Repeat Unit Structure on the Glass Transition-Nanoconfinement Effect and the Cooperativity Length Scale. *Macromolecules* **2005**, *38*, 1767–1778.
25. Reiter, G. Mobility of Polymers in Films Thinner Than Their Unperturbed Size. *Europhys. Lett.* **1993**, *23*, 579–584.
26. Bodiguel, H.; Fretigny, C. Reduced Viscosity in Thin Polymer Films. *Phys. Rev. Lett.* **2006**, *97*, 266105.
27. Xavier, J. H.; Li, C.; Rafailovich, M. H.; Sokolov, J. C. Dynamics of Ultrathin Films in the Glassy State. *Langmuir* **2005**, *21*, 5069–5072.
28. O'Connell, P. A.; McKenna, G. B. Rheological Measurements of the Thermoviscoelastic Response of Ultrathin Polymer Films. *Science* **2005**, *307*, 1760–1763.
29. Granick, S.; Hu, H.-W. Nanorheology of Confined Polymer Melts. 1. Linear Shear Response at Strongly Adsorbing Surfaces. *Langmuir* **1994**, *10*, 3857–3866.
30. Peanasky, J.; Cai, L. L.; Granick, S. Nanorheology of Confined Polymer Melts. 3. Weakly Adsorbing Surfaces. *Langmuir* **1994**, *10*, 3874–3879.
31. Chan, D. Y. C.; Horn, R. G. The Drainage of Thin Liquid Films Between Solid Surfaces. *J. Chem. Phys.* **1985**, *83*, 5311–5324.
32. Israelachvili, J. N. Measurements of the Viscosity of Thin Fluid Films Between Two Surfaces With and Without Adsorbed Polymers. *Colloid Polym. Sci.* **1986**, *264*, 1060–1065.
33. Hu, H.-W.; Granick, S. Viscoelastic Dynamics of Confined Polymer Melts. *Science* **1992**, *258*, 1339–1342.
34. Gacoin, E.; Fretigny, C.; Chateauminois, A.; Perriot, A.; Barthel, E. Measurement of the Mechanical Properties of Thin Films Mechanically Confined within Contacts. *Tribol. Lett.* **2006**, *21*, 245–252.
35. VanLandingham, M. R.; Villarrubia, J. S.; Guthrie, W. F.; Meyers, G. F. Nanoindentation of Polymers: An Overview. *Macromol. Symp.* **2001**, *167*, 15–43.
36. Pethica, J. B.; Hutchings, R.; Oliver, W. C. Hardness Measurements at Penetration Depths as Small as 20-nm. *Philos. Mag. A* **1983**, *48*, 593–606.
37. Cross, G. L. W.; Rowland, H. D.; O'Connell, B. S.; King, W. P.; Pethica, J. B. Variable Temperature Thin Film Nanoindentation with a Flat Punch. *Rev. Sci. Instrum.* **2008**, *79*, 013904.
38. Engmann, J.; Servais, C.; Burbidge, A. S. Squeeze Flow Theory and Applications to Rheometry: A Review. *J. Non-Newtonian Fluid Mech.* **2005**, *132*, 1–27.
39. Macosko, C. M. *Rheology: Principles, Measurements, and Applications*; Wiley-VCH: New York, 1994; p 550.
40. Quinson, R.; Perez, J.; Rink, M.; Pavan, A. Yield Criteria for Amorphous Glassy Polymers. *J. Mater. Sci.* **1997**, *32*, 1371–1379.
41. Richeton, J.; Ahzi, S.; Vecchio, K. S.; Jiang, F. C.; Adharapurapu, R. R. Influence of Temperature and Strain Rate on the Mechanical Behavior of Three Amorphous Polymers: Characterization and Modeling of the Compressive Yield Stress. *Int. J. Solids Struct.* **2006**, *43*, 2318–2335.
42. Ding, Y.; Ro, H. W.; Germer, T. A.; Douglas, J. F.; Okerberg, B. C.; Karim, A.; Soles, C. L. Relaxation Behavior of Polymer Structures Fabricated by Nanoimprint Lithography. *ACS Nano* **2007**, *1*, 84–92.
43. Tanguy, A.; Leonforte, F.; Barrat, J.-L. Plastic response of a 2D Lennard-Jones Amorphous Solid: Detailed Analysis of the Local Rearrangements at Very Slow Strain Rate. *Eur. Phys. J. E* **2006**, *20*, 355–364.
44. Haward, R. N. *The Physics of Glassy Polymers*, 2nd ed.; Applied Science Publishers Ltd.: New York, 1997; p 620.
45. Robertson, R. E. Theory for the Plasticity of Glassy Polymers. *J. Chem. Phys.* **1966**, *44*, 3950–3956.
46. Wu, J. J.; Buckley, C. P. Plastic Deformation of Glassy Polystyrene: A Unified Model of Yield and the Role of Chain Length. *J. Polym. Sci. B: Polym. Phys.* **2004**, *42*, 2027–2040.
47. Dieter, G. E. *Mechanical Metallurgy*, 3rd ed.; McGraw-Hill: London, 1988.
48. Stevens, J. R.; Coakley, R. W.; Chau, K. W.; Hunt, J. L. The Pressure Variation of the Glass Transition Temperature in Atactic Polystyrene. *J. Chem. Phys.* **1986**, *84*, 1006–1014.
49. Xavier, J. H.; Pu, Y.; Li, C.; Rafailovich, M. H.; Sokolov, J. Transition of Linear to Exponential Hole Growth Modes in Thin Free-Standing Polymer Films. *Macromolecules* **2004**, *37*, 1470–1475.
50. Hieber, C. A.; Chiang, H. H. Some Correlations Involving the Shear Viscosity of Polystyrene Melts. *Rheol. Acta* **1989**, *28*, 321–332.
51. Tsenoglou, C. Non-Newtonian Rheology of Entangled Polymer Solution and Melts. *Macromolecules* **2001**, *34*, 2148–2155.
52. Lyulin, A. V.; Balabaev, N. K.; Mazo, M. A.; Michels, M. A. J. Molecular Dynamics Simulation of Uniaxial Deformation of Glassy Amorphous Atactic Polystyrene. *Macromolecules* **2004**, *37*, 8785–8793.
53. Ferry, J. D. *Viscoelastic Properties of Polymers*, 3rd ed.; John Wiley & Sons: New York, 1980; p 641.
54. Miyazaki, T.; Nishida, K.; Kanaya, T. Thermal Expansion Behavior of Ultrathin Polymer Films Supported on Silicon Substrate. *Phys. Rev. E* **2004**, *69*, 061803-1–061803-6.
55. Lin, Y. Y.; Hui, C.-Y.; Conway, H. D. A Detailed Elastic Analysis of the Flat Punch (Tack) Test for Pressure-Sensitive Adhesives. *J. Polym. Sci. B: Polym. Phys.* **2000**, *38*, 2769–2784.
56. Yang, F. Asymptotic Solution to Axisymmetric Indentation of a Compressible Elastic Thin Film. *Thin Solid Films* **2006**, *515*, 2274–2283.
57. Pethica, J. B.; Oliver, W. C. *Materials Research Society Symposium Proceedings*; Materials Research Society: Warrendale, PA, 1989; Vol. 130, p 13.